Self-assembly of a diferrous triple-stranded helicate with bis(2,2'-bipyridine) ligands: Thermodynamic and kinetic intermediates

N. Fatin-Rouge, Sylvie Blanc, E. Leize, Alain van Dorsselaer, Paul Baret, Jean-Louis Pierre, Anne-Marie Albrecht-Gary

Self-Assembly of a Diferrous Triple Stranded Helicate with Bis(2,2'-Bipyridine) Ligands : Thermodynamic and Kinetic Intermediates

Nicolas Fatin-Rouge, Sylvie Blanc, Emmanuelle Leize, Alain Van Dorsselaer, Paul Baret, Jean-Louis Pierre, and Anne-Marie Albrecht-Gary*

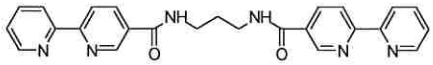

Strand **L**

We present a speciation study of mono- and diferrous complexes formed with ligand **L**. A combination of ESMS, potentiometry and spectrophotometry led to the characterization of three complexes, $\mathbf{L}_2Fe^{2+}$, $\mathbf{L}_2Fe_2^{4+}$ and $\mathbf{L}_3Fe_2^{4+}$. The flexibility of ligand **L** was confirmed by ^1H NMR and molecular modelling. The dissociation process of $\mathbf{L}_3Fe_2^{4+}$ by OH^- occurred via two rate-limiting steps and revealed the formation of a monoferrous intermediate $\mathbf{L}_3Fe^{2+}$. Taking into account the structural, thermodynamic and kinetic features, we propose a stepwise self-assembling process of the diferrous triple stranded helicate $\mathbf{L}_3Fe_2^{4+}$.

Self-Assembly of a Diferrous Triple Stranded Helicate with Bis(2,2'-Bipyridine) Ligands : Thermodynamic and Kinetic Intermediates

Nicolas Fatin-Rouge,[†] Sylvie Blanc,[†] Emmanuelle Leize,[§] Alain Van Dorsselaer[§], Paul Baret,[‡] Jean-Louis Pierre,[‡] and Anne-Marie Albrecht-Gary,[†]*

Contribution from the Laboratoire de Physico-Chimie Bioinorganique, UMR 7509 du CNRS, Faculté de Chimie, 1 rue Blaise Pascal, 67000 Strasbourg, France, the Laboratoire de Spectrométrie de Masse Bioorganique, UMR 7509 du CNRS, Faculté de Chimie, 1 rue Blaise Pascal, 67000 Strasbourg, France and the Laboratoire de Chimie Biomimétique, UMR 5616 du CNRS, 301 rue de la Chimie, 38041 Grenoble, France.

Submitted as an Article to

Journal of Inorganic Chemistry

[†] Laboratoire de Physico-Chimie Bioinorganique.

[§] Laboratoire de Spectrométrie de Masse Bioorganique.

[‡] Laboratoire de Chimie Biomimétique.

* To whom correspondence should be addressed.

e-mail: amalbre@chimie.u-strasbg.fr

Abstract:

The protonation and iron(II) coordination properties of a bis(2,2'-bipyridine) ligand **L** were investigated in methanol. The protonated forms showed allosteric effects due to the flexibility of the strand. Speciation studies of the corresponding ferrous complexes were carried out as a function of p[H] and iron(II) concentrations. A combination of electrospray mass spectroscopy, potentiometry and spectrophotometry allowed the determination in solution of three ferrous complexes, one mononuclear ($\mathbf{L}_2Fe^{2+}$) and two dinuclear ($\mathbf{L}_2Fe_2^{4+}$ and $\mathbf{L}_3Fe_2^{4+}$) species. Their structure was deduced from the metal spin–state and confirmed by ^1H NMR measurements and molecular modeling. The dissociation process of the triple stranded diferrous helicate $\mathbf{L}_3Fe_2^{4+}$ by OH^- revealed two rate-limiting steps. The former leads to the formation of a monoferrous triple stranded compound via a classical mechanism, which involves hydroxy-ferrous complexes. A similar process was observed in the latter step for the release of the ferrous cation from the mononuclear intermediate. Taking into account the structural, thermodynamic and kinetic features provided by the present study, we could propose a self-assembling mechanism of the triple stranded diferrous helicate.

Introduction

Metal-directed self-assembly processes leading to double or triple polynuclear helices attracted considerable attention over the past ten years.[1-5] In the ferrous helicate family Serr et al.[6] and Youinou et al.[7] measured by electrochemistry the interactions between the two iron(II) centers in double or triple helical complexes. Zelikovich et al.[8] determined the oxidation properties of a monoferrous anchored triple stranded complex, a model of the iron(II) cavity for redox switches. Takenaka et al.[9] exploited the iron(II) complexation properties to form a double helix with a bipyridine ligand carrying a functional nucleotide used for DNA hybridization. Lieberman and Sasaki[10] synthesized a three α-helix bundle protein using a tris(bipyridine) metal complex as a template to provide a well-defined model system to study metalloenzymes functions. A true dinuclear triple-helical arrangement, which is generated by three ligands with two bidentate units, linked by a spacer and which complex cations in an octahedral geometry, needs the homochirality of the two coordination sites.[1] Recent studies combining electrospray mass spectrometry (ES-MS)[11-15] and spectrophotometric or potentiometric titrations [16-19] constitute the best approach for the elaboration of a chemical model for the self-assembly process. Thermodynamic and kinetic studies on a flexible strand **L** (Figure 1) which is able to form a homochiral $\mathbf{L}_3Fe_2$ dinuclear iron(II) complex, as previously characterized,[20] were undertaken for a better understanding of the self-assembling process.

Figure 1

Classical potentiometric and spectrophotometric titrations in combination with ES-MS and ^{1}H NMR allowed us to determine the nature of the ferrous species, to measure their respective stability constants and absorption spectra, and to characterize their structure in agreement with modeling calculations. The dissociation studies of the triple stranded

diferrous helicate by hydroxide ions provided informations on the lability and accessibility of the two coordination sites of the helical arrangement.

Experimental Section

NMR. The ^{1}H NMR spectra were recorded at 25 °C on a Bruker AM 360 spectrometer. Chemical shifts are reported in parts per million with respect to TMS. Titration of ligand **L** (10^{-3} M) was performed in CD_3OD (Armar, Methanol-d_4, 99%) in order to compare our results with those obtained by potentiometry in the same solvent. Trifluoroacetic acid (Fluka, 98%) was used for p[D] adjustments of the solutions. Measurements were made on a Metrohm Titrino 736 GP millivoltmeter using a combined glass electrode (Metrohm) prepared and standardized in methanol. Previous ^{1}H NMR studies have been done on the ferrous helicate $\mathbf{L}_3Fe_2^{4+}$ in water.[20] CD_3CN (Armar, Acetonitrile-d_3, 99.8) was chosen as a polar, but not protic solvent, to analyze the structure of the diferrous triple stranded complex (10^{-3} M) in solution.

ES MS. Positive ES mass spectra were recorded on a Quattro II triple quadrupole mass spectrometer (Micromass, Altrincham, UK) scanning over the m/z range 200-2200 in 15 seconds. 10 scans were added to produce the final data. The samples were introduced in the ES source with a flow rate of 5 µl/min. The extraction cone potential was set at 40 V in order to avoid any fragmentation. Mass scale calibration employed the multiply charged ions series from horse heart myoglobin. Only average masses were measured. Assignment of ions was confirmed checking their isotopic distribution. ES mass spectra analysis gave information on the stoichiometry of the ferrous species formed. Free ligand **L** was titrated as a function of [Fe(II)] ($FeSO_4$,7 H_2O, Aldrich, p.a.) in pure methanol (Merck, p.a.) and then the concentrations of ligand **L** and Fe(II) ($[\mathbf{L}]_{tot} = 5.10 \times 10^{-5}$ M; $[Fe(II)]_{tot} = 2.55 \times 10^{-5}$ M) were

fixed at two values of p[H] (2.50; 10.20) using respectively perchloric acid (Prolabo, normapur, 70% min) or lithium methylate (Fluka, purum).

Molecular Mechanics Calculations. Molecular modeling calculations on ligand **L** were carried out using Hyperchem, version 5.0.[21] Geometry optimization was obtained by the MM^+ method with a convergence criteria equal to 0.01. The charge repartitions were calculated by the semi-empirical AM1 method[22] with a gradient of convergence fixed to 0.05.

Spectrophotometry and Potentiometry. All the solutions were prepared with dried methanol of spectral quality grade (Merck, p.a.) deoxygenated by the flux of oxygen free argon and purified by a Sigma Oxiclear cartridge. The ionic strength was adjusted to 0.1 with tetrabutylammonium trifluoromethanesulfonate (Fluka, puriss). Stock solutions of bis(2,2'-bipyridine) ligand **L**, synthesized as previously described,[20] were prepared by quantitative dissolution of solid samples. Fresh stock ferrous sulfate solutions (10^{-2} M, $FeSO_4$,7 H_2O, Aldrich, p.a.) were titrated by 2,2'-bipyridine (Sigma) in methanol:water (50:50 by volume) in the presence of hydroxylamine[23] at 520nm ($\varepsilon_{520\ nm} = 9550\ M^{-1}\ cm^{-1}$). Perchloric acid solutions (Prolabo, normapur, 70% min) were titrated by NaOH (10^{-1} M, Carlo Erba, Titrisol normex) with phenolphtalein as an indicator and prepared just before use. Hydrogen ion concentrations were measured with a combined glass electrode (Ingold, high alkalinity). The Ag/AgCl reference electrode was filled with tetrabutylammonium chloride (0.05 M, Fluka, p.a.) and tetrabutylammonium trifluoromethanesulfonate (0.05 M, Fluka, p.a.) in pure methanol saturated with silver perchlorate (Merck, p.a.). Potential differences were given by a Tacussel Isis 20,000 millivoltmeter. The linearity of the glass electrode was verified using solutions with known hydrogen ion concentrations in methanol[24-26] at I = 0.1 M with tetrabutylammonium chloride (Fluka, p.a.). The titration of the free ligand (40 ml, 1.00×10^{-4} M) was carried out in a jacketed cell (Metrohm) maintained at 25.0 (2)°C by the flow of a Lauda thermostat. The initial p[H] was adjusted to 10.25 by lithium methylate (Fluka, purum)

and the solution was then titrated by perchloric acid to p[H] 2.67. A small sample (500 μL) was taken after each addition of acid, and simultaneous p[H] and UV-visible measurements were recorded between 250 nm and 650 nm using a Kontron Uvikon 941 spectrophotometer and Hellma quartz optical cells (0.2 cm) maintained at 25.0 (2)°C by the flow of a Lauda thermostat.

Batch titrations of ligand **L** with iron(II) were undertaken in a 5 ml flask. p[H] was fixed to 3.50 using 4-toluene sulfonic acid and the total concentration of ligand **L** to 5.0×10^{-5} M. The $[Fe(II)]_{tot}/[\mathbf{L}]_{tot}$ ratio was varying between 0 and 3.5. In another experiment, $[\mathbf{L}]_{tot}$ was fixed to 5.1×10^{-5} M and $[Fe(II)]_{tot}$ to 2.5×10^{-5} M and p[H] values were in a span between 10.27 to 2.55 using perchloric acid. The stability of each solution was carefully checked. The corresponding UV-visible spectra were recorded (250 nm - 650 nm) on a Kontron Uvikon 941 spectrophotometer using Hellma quartz optical cells (0.2 cm or 2 cm). An example of the spectral evolution of ligand **L** at p[H] = 3.50 as a function of the concentrations of iron(II) is given in Figure 2.

Figure 2

The corresponding spectrophotometric data for ligand **L** in the absence and in the presence of iron(II) were processed versus p[H] with both the Letagrop-Spefo[27-31] and Specfit[32-34] programs, which adjust either the protonation or the stability constants and the absorptivities of the species formed at equilibrium. Letagrop-Spefo[27-31] uses the Newton-Raphson algorithm to solve mass balance equations and a pit-mapping method to minimize the errors and determine the best values of the parameters. Specfit[32-34] uses factor analysis to reduce the absorbance matrix and to extract the eigenvalue prior to the multiwavelength fit of the reduced data set according to the Marquardt algorithm.[35,36] Distribution curves of the various species were obtained using the Haltafall[37] program.

Dissociation kinetics. The kinetics of ferrous helicate dissociation by hydroxide ions was investigated using spectrophotometry. The dinuclear triple helix ([**L**] = 2.5×10^{-4} M, $Fe(II)_{tot} = 1.2 \times 10^{-4}$ M) was prepared at p[H] = 9.5 and the concentration of the tetrabutylammonium hydroxide (Fluka, puriss) used as a nucleophile reagent was at least 40 times higher than the complex concentration to ensure pseudo-first order conditions with respect to the ferrous complex. Equal volumes of each reactant, previously thermostated at 25.0 (2)°C, were successively introduced into 0.5 cm pathlength quartz cells (Hellma). The reaction was followed by spectrophotometry at 520 nm on a Kontron Uvikon 941 spectrophotometer thermostated at 25.0 (2)°C by the flow of a Lauda thermostat.
The kinetic data were processed with the Biokine software[38], which uses the Simplex algorithm.[39] The rate constants were determined with the help of the commercial Enzfitter program,[40] based on Marquardt analysis.[35-36] Time-resolved absorption spectra were also collected between 220 and 620 nm with one cm pathlength for $[OH^-] = 9.8 \times 10^{-4}$ M. The rate constants and extinction coefficients were adjusted to the multiwavelength data sets by nonlinear least-squares analysis with the Specfit program.[32-34] (Supporting Information).

Results

NMR. ^{1}H NMR titration of ligand **L** in deuterated methanol (Figure 3) indicates a $_{C2}$ symmetry of the $\mathbf{L}H^+$ and $\mathbf{L}H_2^{2+}$ species due to the equivalence of the 2,2'-bipyridine moieties. Protons $H_{5'}$ and $H_{6'}$, which are the most affected by p[D] changes, indicate that the protonation occurs on the external pyridine of the 2,2'-bipyridine subunits (Figure 1).
^{1}H NMR shifts of the ferrous helicate measured in CD_3CN are given in Supporting Information. As previously described,[20] the central methylene groups of the spacer, act as spectroscopic probes for symmetry and structure determination of the $\mathbf{L}_3Fe_2^{4+}$ complex.

Figure 3

ES-MS. The pseudomolecular ions of the different species observed by ESMS are given in Supporting Information at p[H] = 2.50 and 10.20 for a given [Fe(III)]/$[L]_{tot}$ ratio and at three different metal to ligand ratios in pure methanol. Ionization of the ferrous complexes was performed by the loss of the counter-ions either ClO_4^- or SO_4^{2-}. The mass spectrometric study clearly showed the formation of four ferrous complexes, two mononuclear species with one and two ligands ($\mathbf{L}Fe^{2+}$ and $\mathbf{L}_2Fe^{2+}$) and two dinuclear complexes with two and three ligands ($\mathbf{L}_2Fe_2^{4+}$ and $\mathbf{L}_3Fe_2^{4+}$).

Potentiometry and Spectrophotometry. The statistical treatment [27-30, 32-34] of the data provided by a spectrophotometric titration of ligand lead to a model with three absorbing acid-base species: a deprotonated ligand **L**, a mono- and a diprotonated species respectively $\mathbf{L}H^+$ and $\mathbf{L}H_2^{2+}$. The corresponding protonation constants are given in (Table 1).

The successive protonations of ligand **L** induce a bathochromic shift (10 nm -20 nm) of the absorption band centered at 291 nm as shown in Supporting Information

Table 1

A metal to ligand charge transfer band at 540 nm is observed with the formation of ferrous complexes (Figure 2). A model involving three ferrous species $\mathbf{L}_2Fe^{2+}$, $\mathbf{L}_2Fe_2^{4+}$ and $\mathbf{L}_3Fe_2^{4+}$, detected by ESMS was fitted by statistical methods.[27-30, 32-34] The values of the corresponding stability constants are given in Table 1, and the respective electronic spectra are presented in Supporting Information.

Dissociation kinetics. The dissociation process of the diferrous helicate under basic conditions was investigated. The corresponding global reaction is written:

$$\mathbf{L}_3Fe_2^{4+} + 2n(OH^-) \rightarrow 3\ \mathbf{L} + 2Fe(OH)_n^{(2-n)+} \qquad [1]$$

A biexponential decrease of the absorbance at 520 nm (Supporting Information) was recorded versus time. The values of the two corresponding pseudo-first order rate constants $k_{1,obs}$ and

$k_{2,obs}$ were calculated with the Biokine commercial software.[38] Their variation with increasing hydroxide concentrations in excess is presented in Figure 4.

Figure 4

The time change of the absorption spectra (220 nm – 620 nm) has been analyzed. A biexponential signal was confirmed and the spectrophotometric characterization of a single intermediate was provided. Its absorption band centered at 540 nm corresponds to a metal to ligand charge transfer band which is characteristic of a tris-bipyridine ferrous species. The value of the maximum extinction coefficient is half of that determined for the diferrous helicate (**Table 4**). These observations support the formation of L_3Fe^{2+} as an intermediate in the biexponential dissociation process of $L_3Fe_2^{4+}$.

According to the classical mechanism[41,42] proposed for the dissociation of tris(diimine) iron(II) complexes by nucleophilic scavengers as OH^- and CN^-, we propose a reaction scheme (Table 2) which takes into account the fast formation of ion pairs between the diferrous $\mathbf{L}_3Fe_2$ and monoferrous $\mathbf{L}_3Fe$ species (and respectively one [$\mathbf{L}_3Fe_2(OH)$, $\mathbf{L}_3Fe(OH)$] and two [$\mathbf{L}_3Fe_2(OH)_2$, $\mathbf{L}_3Fe(OH)_2$] hydroxide anions). The faster step concerns the diferrous triple stranded complex and the slower one the monoferrous corresponding species.

Former step

$$\mathbf{L}_3Fe_2 + OH \underset{\leftarrow}{\overset{K_1}{\rightarrow}} \mathbf{L}_3Fe_2(OH) \qquad [2]$$

$$\mathbf{L}_3Fe_2(OH) + OH \underset{\leftarrow}{\overset{K_2}{\rightarrow}} \mathbf{L}_3Fe_2(OH)_2 \qquad [3]$$

$$\mathbf{L}_3Fe_2(OH)_2 \xrightarrow{k_3} \mathbf{L}_3Fe + Fe(OH)_2 \qquad [4]$$

$$\mathbf{L}_3Fe_2 \xrightarrow{k_{d,\mathbf{L}_3Fe_2}} \mathbf{L}_3Fe + Fe \qquad [5]$$

Latter step

$$\mathbf{L}_3Fe + OH \underset{\leftarrow}{\overset{K_4}{\rightarrow}} \mathbf{L}_3Fe(OH) \qquad [6]$$

$$\mathbf{L}_3\mathrm{Fe(OH)} + \mathrm{OH} \underset{\longleftarrow}{\xrightarrow{K_5}} \mathbf{L}_3\mathrm{Fe(OH)_2} \quad [7]$$

$$\mathbf{L}_3\mathrm{Fe(OH)_2} \xrightarrow{k_6} 3\mathbf{L} + \mathrm{Fe(OH)_2} \quad [8]$$

$$\mathbf{L}_3\mathrm{Fe} \xrightarrow{k_{d,L_3Fe}} 3\,\mathbf{L} + \mathrm{Fe} \quad [9]$$

Our kinetic data were processed by statistical methods[40] and follow the following rate equations [10] and [11]

$$-\frac{d}{dt}[\mathbf{L}_3\mathrm{Fe}_2] = k_{1,obs} \times [\mathbf{L}_3\mathrm{Fe}_2] \quad [10]$$

$$-\frac{d}{dt}[\mathbf{L}_3\mathrm{Fe}] = k_{2,obs} \times [\mathbf{L}_3\mathrm{Fe}] \quad [11]$$

With $[\mathbf{L}_3\mathrm{Fe}_2]_{tot} = [\mathbf{L}_3\mathrm{Fe}_2] + [\mathbf{L}_3\mathrm{Fe}_2(\mathrm{OH})] + [\mathbf{L}_3\mathrm{Fe}_2(\mathrm{OH})_2]$ [12]

and $[\mathbf{L}_3\mathrm{Fe}]_{tot} = [\mathbf{L}_3\mathrm{Fe}] + [\mathbf{L}_3\mathrm{Fe(OH)}] + [\mathbf{L}_3\mathrm{Fe(OH)_2}]$ [13]

Using these equations, the variations of $k_{1,obs}$ and $k_{2,obs}$ versus the concentrations of hydroxide anions are given by the respective relationships [14] and [15]:

$$k_{1,obs} = \frac{k_3 \times K_1 \times K_2[OH]^2}{1 + K_1[OH] + K_1 \times K_2[OH]^2} \quad [14]$$

$$k_{2,obs} = \frac{k_6 \times K_4 \times K_5[OH]^2}{1 + K_4[OH] + K_4 \times K_5[OH]^2} \quad [15]$$

The thermodynamic constants K_1, K_2, K_3 and K_4 related to the formation of mono- and dihydroxy species as well as the rate constants k_3 and k_6 which correspond to the two dissociation limiting steps were determined and their values are presented in Table 2.

Table 2

Discussion

Acid-Base Properties of Ligand L. The 2,2'-bipyridine moiety has two nitrogen atoms which can be protonated, and its log K_1 value respectively in water[43] and in methanol:water[43] (87.9% by weight), indicates a strong decrease of about one order of magnitude in the

presence of methanol (Table 3). Various studies[44,45] also pointed out the influence of the nature and of the position of the substituents to explain variations of log K_1 (Table 3). The presence of an amide group in the five position of ligand **L** (Figure 1), according to the data presented in Table 3, should decrease the value of log K_1. Our result (log K_1 = 4.54 (4)) does not obey to these trends.

Table 3

The ^{1}H NMR data clearly show a high symmetry of the LH^+ form. This result is consistent with a folding of the flexible strand **L** around a single proton coordinated by the two 2,2'-bipyridine subunits (Figure 3). This observation was confirmed by molecular modeling calculations with Hyperchem,[21] which showed that the best stable conformation in vacuum was a folded structure with stacking interactions between the two aromatic moieties (Figure 5). The coordination of protons by more than one diimine ligand has also previously been found under different experimental conditions by several authors.[46,47] The $\log K_2$ value relative to ligand **L** ($\log K_2$ = 3.6 (1)) is identical, within the experimental errors, to the $\log K_1$ value reported for 2,2'-bipyridine in methanol[43] (Table 3). This similarity indicates the unfolding of the molecule and the absence of interactions between the two protons in ligand **L**. In the p[H] span investigated in this study, it was not possible to observe tri or tetraprotonated forms of ligand **L**. These further protonations are expected in agreement with the second protonation[48-50] of the two 2,2'-bipyridine moieties (log K_2 = 0.2).

Figure 5

For the sake of comparison, the absorption maxima of the different protonated species of ligand **L** and 2,2'-bipyridine were gathered in Table 4. In the solid state, in organic solvents and in basic solutions, 2,2'-bipyridine exists in a trans conformation in agreement with theoretical calculations.[51] Its electronic spectrum consists of a major band with a maximum at 280 nm ($\varepsilon_{280} = 1.3 \times 10^4$ M^{-1} cm^{-1}) generally assigned to the transition of an electron from the

highest occupied π to the lowest unoccupied π* molecular orbital.[52] The wavelength of maximal absorbance remained unchanged in methanol, but showed higher intensity.[53-55] The calculated electronic spectrum of **L** ($\varepsilon_{291} = 4.52 \times 10^4$ M^{-1} cm^{-1}) is in good agreement with these observations. The monoprotonated 2,2'-bipyridine has a cis conformation, stabilized by a cationic hydrogen bond. Its absorption band in the UV corresponding to π→π* transitions ($\varepsilon_{302} = 1.58 \times 10^4$ M^{-1} cm^{-1}) is shifted of about 20 nm towards longer wavelengths and its intensity increases compared with the free 2,2'-bipyridine[55] ($\varepsilon_{280} = 1.3 \times 10^4$ M^{-1} cm^{-1}). The same red shift of the π→π* ligand band of **L** ($\varepsilon_{291} = 4.52 \times 10^4$ M^{-1} cm^{-1}) and a decrease of the absorptivity ($\varepsilon_{305} = 3.97 \times 10^4$ M^{-1} cm^{-1}) were observed for $\mathbf{LH}^+$ and confirm that the proton is bound by both 2,2'-bipyridine subunits with a nearly cis conformation. The transition from a cis conformation of the monoprotonated 2,2'-bipyridine to a trans conformation in the diprotonated form, in order to reduce both steric hindrance and electrostatic repulsions, induces a large shift (12 nm) towards shorter wavelengths.[55] In our bis(2,2'-bipyridine) ligand, no significant change neither in wavelength nor in absorptivity is induced by the second protonation (Table 4). This result suggests that a cis conformation is kept in the folded monoprotonated species as well as in the diprotonated species $\mathbf{LH_2}^{2+}$ with two monoprotonated 2,2'-bipyridine moieties.

Table 4

Ferrous Complexes Characterization. Depending on the p[H] and on the $[Fe(II)]_{tot}/[\mathbf{L}]_{tot}$ ratio, three major ferrous complexes $\mathbf{L_2Fe}^{2+}$, $\mathbf{L_2Fe_2}^{4+}$ and $\mathbf{L_3Fe_2}^{4+}$ were observed at equilibrium by potentiometry, absorption spectrophotometry (Figure 6) and ESMS. 2,2'-bipyridine is able to form high-spin and low-spin complexes with different transition metal ions.[43] The consecutive formation constants for iron(II) 2,2'-bipyridine complexes were reported to follow in water the sequence[56] $K_{(2,2'\text{-bipyridine})Fe(II)}$ (1.6×10^4 M^{-1}) >

$K_{(2,2'\text{-bipyridine})_2Fe(II)}$ (5×10^3 M^{-1}) << $K_{(2,2'\text{-bipyridine})_3Fe(II)}$ (3.5×10^9 M^{-1}). The classical decrease of the successive constants[57] was not observed and this anomaly was attributed to spin-pairing on addition of the third 2,2'-bipyridine.[56] This is consistent with the sequence of stability and an increase of the stability of the low-spin tris complex compared to the high-spin mono and bis complexes. Moreover theoretical considerations on tris(α-diimine)iron(II) electronic structures reveal that a π-back donation takes place in the ground state and, as a result, unusually stable complexes of iron(II) are formed.[58]

The electronic spectra of monoferrous $\mathbf{L}_2Fe^{2+}$ and diferrous $\mathbf{L}_2Fe_2^{4+}$ complexes display a metal to ligand charge transfer band centered at 540 nm (Table 4). The intense absorption band at 500 nm,[59,60] characteristic of tris(2,2'-bipyridine) ferrous complexes, was proved to be due to charge transfer transitions from the 3d atomic orbital of iron(II) to the lowest vacant π molecular orbital of the ligand.[61] This band obscures d-d transitions of the metal, but can be distinguished from the $\pi \rightarrow \pi^*$ transition bands of 2,2'-bipyridine at around 300 nm.[52,62] In high-spin octahedral iron(II) complexes, broad $^5T_{2g} \rightarrow {}^5E_g$ transitions occur in the visible/near IR region (900 nm -1200 nm).[63] The absorption spectra that we obtained for $\mathbf{L}_2Fe^{2+}$ and $\mathbf{L}_2Fe_2^{4+}$, then clearly indicate the coordination of three 2,2'-bipyridine fragments. The only structure which can be proposed for $\mathbf{L}_2Fe^{2+}$ is the coordination of two 2,2'-bipyridine functions provided by a folded ligand **L,** the third 2,2'-bipyridine coordination site being brought by a second extended strand **L** (Figure 7). From $\mathbf{L}_2Fe^{2+}$ to $\mathbf{L}_2Fe_2^{4+}$, the addition of a second ferrous cation does not significantly affect the characteristic absorption band in the visible region of the low spin $\mathbf{L}_2Fe^{2+}$ complex. This observation strongly suggests the coordination of the second ferrous cation on the free 2,2'-bipypridine moiety of the extended strand **L** in $\mathbf{L}_2Fe^{2+}$, since the formation of a mono(2,2'-bipyridine) high-spin ferrous complex cannot be detected in the visible region, but at longer wavelengths[63]. The structure that we

propose for the thermodynamic $\mathbf{L}_2Fe^{2+}$ and $\mathbf{L}_2Fe_2^{4+}$ species, agrees well with both the spectrophotometric data and the sequence of stability observed for ferrous 2,2'-bipyridine complexes, since it does not imply the thermodynamic unfavorable ferrous species with two 2,2'-bipyridine coordination sites. The helical structure of $\mathbf{L}_3Fe_2^{4+}$ was established by ^1H NMR[20] measurements (Supporting Information).

Using the protonation and stability constants (Table 1), distribution curves (Figure 6) were calculated under our experimental conditions. Figure 6a illustrates the competition between Fe(II) and H^+ for ligand **L** and shows that $\mathbf{L}_2Fe^{2+}$ and the triple stranded dinuclear helicate are the major species formed at p[H] > 4 for a $[Fe(II)]_{tot}/[\mathbf{L}]_{tot}$ ratio equal to 0.5. Figure 6b reveals the presence of both complexes $\mathbf{L}_3Fe_2^{4+}$ and $\mathbf{L}_2Fe_2^{4+}$. When the ferrous cation is in excess, the helical complex $\mathbf{L}_3Fe_2^{4+}$ is destroyed in favor of $\mathbf{L}_2Fe_2^{4+}$.

Figure 6

Ferrous Helicate Dissociation. Two rate-limiting steps depending on hydroxide anions are involved in the dissociation mechanism of the diferrous helicate $\mathbf{L}_3Fe_2^{4+}$ (Figure 4). The former one leads to the release of a ferrous cation and to the corresponding monoferrous intermediate complex (Table 2). The latter follows an identical mechanism, which gives three free strands and iron(II) (Table 2). The two rate-limiting steps respectively correspond to the attack of OH^-, which induces the loss of a 2,2'-bipyridine coordination site. In agreement with the data available in literature for the dissociation of tris(2,2'-bipyridine) ferrous complexes,[64,65] the two rate limiting steps could be associated with the loss of the first 2,2'-bipyridine units induced by the substitution of two hydroxide anions in each coordination site of the diferrous helicate. These two rate-limiting steps are related to the change from inert low-spin tris(2,2'-bipyridine) to labile high-spin bis and mono(2,2'-bipyridine) ferrous species.[63] This mechanism points out the important role of the kinetic intermediate $\mathbf{L}_3Fe^{2+}$ formed after the former dissociation step. Concerning the OH^- independent pathway of the

diferrous helicate $\mathbf{L}_3Fe_2^{4+}$ and the monoferrous species $\mathbf{L}_3Fe^{2+}$, the respective values of the rate constants $k_{d,\mathbf{L}_3Fe_2^{4+}}$ ($4 \pm 2 \times 10^{-4} s^{-1}$) and $k_{d,\mathbf{L}_3Fe^{2+}}$ ($7 \pm 2 \times 10^{-5}$ s^{-1}) are of the same order of magnitude as found by Basolo et al.[66] for iron(II) tris(2,2'-bipyridine) complexes in water ($1.4 \times 10^{-4} s^{-1}$). This comparison shows similar coordination arrangements between the helical diferrous complex $\mathbf{L}_3Fe_2^{4+}$ and the monoferrous kinetic intermediate $\mathbf{L}_3Fe^{2+}$, both species being very similar in terms of inertness and accessibility to a tris(2,2'-bipyridine) ferrous complex. For the OH^- independent pathway, the successive stability constants calculated for the ion pair formation (Table 2) between the ferrous complex and respectively one hydroxide ($K_1 = 2.2$ (5) M^{-1}; $K_4 = 3.1$ (7) M^{-1}) and two hydroxides ($K_2 = 18$ (4) M^{-1}; $K_5 = 16$ (4) M^{-1}) indicate a large similarity between the two coordination sites of the helicate which remains during the successive release of the two diferrous cations. The values of the rate constant k_3 = (0.19 (4) s^{-1}) and k_6 (4.9 (9) $\times 10^{-2}$ s^{-1}) respectively related to the diferrous and monoferrous species slightly differ of a factor of about five and are of the same order of magnitude as the corresponding rate constant found for the OH^- dependent dissociation of the ferrous tris(phenanthroline) complex in water (4.2×10^{-2} s^{-1}).[67] This comparison suggests that the dissociation of the dihydroxyferrous intermediates is not very sensitive to the chemical structure of the ligand.

In conclusion, we propose in Figure 7 a self-assembling process of a diferrous triple stranded helicate which is consistent with our thermodynamic and kinetic results and which is in excellent agreement with previous studies on 2,2'-bipyridine ligands.

Figure 7

At equilibrium, a combination of methods (^1H NMR, ESMS, absorption spectrophotometry, potentiometry and molecular mechanics modeling) allowed us to characterize three ferrous complexes $\mathbf{L}_2Fe^{2+}$, $\mathbf{L}_2Fe_2^{4+}$ and the helicate $\mathbf{L}_3Fe_2^{4+}$. The flexibility

of strand **L** enables the formation of a stable monoferrous tris(2,2'-bipyridine) $\mathbf{L}_2Fe^{2+}$ species and explains the presence, in excess of iron(II), of a double stranded diferrous complex $\mathbf{L}_2Fe_2^{4+}$. The folded structure of ligand **L** was energetically minimized by molecular mechanics calculations and explained its acid-base properties. Finally, the kinetic study revealed the formation of a monoferrous triple stranded complex $\mathbf{L}_3Fe^{2+}$ and pointed out the lack of strong interactions between the two ferrous coordination sites in the helicoidal structure, as well as their similarity in terms of coordination geometry, inertness and accessibility.

Acknowledgment. This work has been supported by the Centre National de la Recherche Scientifique (UMR 7509 and 5616, PCV program), the Faculty of Chemistry, University Louis Pasteur, Strasbourg (France) and the University Joseph Fourier, Grenoble (France).

Supporting Information Available: Tables of the ^1H NMR data for $L_3Fe_2^{4+}$ in CD_3CN, ESMS data for ferrous complexes. Figures of absorption spectra of ligand L versus p[H], of the dissociation kinetics of the diferrous helicate and of time-resolved spectra during the basic dissociation process of $\mathbf{L}_3Fe_2^{4+}$. This material is available free of charge via the Internet at http://pubcs.acs.org.

References

(1) Lehn, J.M. *Supramolecular Chemistry: Concepts and Perspectives*, VCH, Weinheim, 1995.

(2) Williams, A. *Chem. Eur. J.* **1997**, *3*, 15-19.

(3) Piguet, C.; Bernardinelli, G.; Hopfgartner, G. *Chem. Rev.* **1997**, *97*, 2005-2062.

(4) Albrecht, M.; Schneider, M.; Frohlich, R. *New J. Chem.* **1998**, *22*, 753-754.

(5) Caulder, D.; Raymond, K. N. *J. Chem. Soc., Dalton Trans.* **1999**, 1185-1200.

(6) Serr, B. R.; Andersen, K. A.; Elliott, C. M.; Anderson, O. P. *Inorg. Chem.* **1988**, *27*, 4499-4505.

(7) Youinou, M. T.; Ziessel, R.; Lehn, J. M. *Inorg. Chem.* **1991**, *30*, 2144-2148.

(8) Zelikovich, L.; Libman, J.; Shanzer, A. *Nature* **1995**, *374*, 790-792.

(9) Takenaka, S.; Funatu, Y.; Kondo, H. *Chem. Letters* **1996**, 891-892.

(10) Lieberman, M.; Sasaki, T. *J. Am. Chem. Soc.* **1991**, *113*, 1470-1471.

(11) Jaquinod, M.; Leize, E.; Potier, N.; Albrecht, A. M.; Shanzer, A.; Van Dorsselaer, A. *Tetrahedron Letters* **1993**, *34*, 2771-2774.

(12) Leize, E.; Van Dorsselaer, A.; Kramer, R.; Lehn, J. M. *J. Chem. Soc., Chem. Commun.* **1993**, 990-993.

(13) Hopfgartner, G.; Piguet, C.; Henion, J. D. *J. Am. Soc. Mass Spectrom.* **1994**, *5*, 748-756.

(14) Leize, E.; Jaffrezic, A.; Van Dorsselaer, A. *J. Mass Spectrom.* **1996**, *31*, 537-544.

(15) Marquis-Rigault, A.; Dupont-Gervais, A.; Baxter, P. N. W.; Van Dorsselaer, A.; Lehn, J. M. *Inorg. Chem.* **1996**, *35*, 2307-2310.

(16) Garrett, T. M.; Koert, U.; Lehn, J. M. *J. Phys. Org. Chem.* **1992**, *5*, 529-532.

(17) Pfeil, A.; Lehn, J. M. *J. Chem. Soc., Chem. Commun.* **1992**, 838-840.

(18) Blanc, S.; Yakirevitch, P.; Leize, E.; Meyer, M.; Libman, J.; Van Dorsselaer, A.; Albrecht-Gary, A. M.; Shanzer, A. *J. Am. Chem. Soc.* **1997**, *119*, 4934-4944.

(19) Piguet, C.; Bünzli, J. C.; Bernardinelli, G.; Hopfgartner, G.; Petoud, S.; Schaad, O. *J. Am. Chem. Soc.* **1996**, *118*, 6681-6697.

(20) Zurita, D.; Baret, P.; Pierre, J. L. *New J. Chem.* **1994**, *18*, 1143-1146.

(21) Hyperchem, 5.0 version, Hypercube Trademarks, **1996**.

(22) Dewar, M. J. S.; Zoebisch, E. V.; Healy, E. F.; Stewart, J. J. P. *J. Am. Chem. Soc.* **1985**, *107*, 3902-3909.

(23) Schilt, A. A.; *Analytical Applications of 1,10-Phenanthroline and Related Compounds,* Pergamon Press **1969**.

(24) Alfenaar, M.; De Ligny, C. L. *Rec. Trav. Chim. Pays-Bas* **1967**, *86*, 1185-1190.

(25) Rorabacher, D. B.; MacKellar, W. J.; Shu, F. R.; Bonavita, S. M. *Anal. Chem.* **1971**, *43*, 561-573.

(26) Commission on Electroanalytical Chemistry *Pure and Appl. Chem.* **1985**, 57, 865-876.

(27) Sillen, L. G.; Warnqvist, B. *Ark. Kemi* **1968**, *31*, 341-351.

(28) Arnek, R.; Sillen, L. G.; Wahlberg, O. *Ark. Kemi* **1968**, *31*, 353-363.

(29) Brauner, P.; Sillen, L. G.; Whiteker, R. *Ark. Kemi* **1968**, *31*, 365-377.

(30) Sillen, L. G. *Acta Chem. Scand.* **1964**, *18*, 1085-1098.

(31) Sillen, L.G.; Warnqvist, B. *Ark. Kemi.* **1968**, *31*, 377-390.

(32) Gampp, H.; Maeder, M.; Meyer, C. J.; Zuberbühler, A. D. *Talanta* **1985**, *32*, 95-101.

(33) Gampp, H.; Maeder, M.; Meyer, C. J.; Zuberbühler, A. D. *Talanta* **1985**, *32*, 257-264.

(34) Gampp, H.; Maeder, M.; Meyer, C. J.; Zuberbühler, A. D. *Talanta* **1986**, *33*, 943-951.

(35) Marquardt, D. W. Q. *J. Soc. Indust. Appl. Math.* **1963**, *11*, 431-441.

(36) Maeder, M.; Zuberbühler A. D. *Anal. Chem.* **1990**, *62*, 2220-2224.

(37) Ingri, N.; Kakolowicz, W.; Sillen, L. G.; Warnqvist, B. *Talanta* **1967**, *14*, 1261-1286.

(38) Bio-Logic Company, Ed. Bio-logic Company, Echirolles, **1991**.

(39) Nelder, J. A.; Mead, R. *The Computer Journal*, **1965**, *7*, 308-313.

(40) Leatherbarrow, J. Ed. Biosoft, Cambridge, **1987**.

(41) Margerum, D. W.; Morgenthaler, L. P. *J. Am. Chem. Soc.* **1961**, *84*, 706-709.

(42) Burgess, J.; Galema, S.A.; Hubbard, C. D. *Polyhedron* **1991**, *10*, 703-709.

(43) McBryde, W. A. E. *IUPAC Chemical Data Series*, **1978**, *17*, 1-79.

(44) Tsai, C. S. *Can. J. Chem.* **1967**, *45*, 2862-2864.

(45) James, B. R.; Lyons, J. R.; Williams, R. J. P. *Biochemistry* **1962**, *1*, 379-385.

(46) Dietrich-Buchecker, C. O.; Sauvage, J. P.; Armaroli, N.; Ceroni, P.; Balzani, V. *New J. Chem.* **1996**, *20*, 801-808.

(47) Fahsel, M. J.; Banks, C. V. *J. Am. Chem. Soc.* **1966**, *88*, 878-884.

(48) McBryde, W. A. E. *Can. J. Chem.* **1965**, *43*, 3472-3476.

(49) Krumholz, P. *J. Am. Chem. Soc.* **1956**, *78*, 87-91.

(50) Westheimer, F. H.; Benfey, O. T. *J. Am. Chem. Soc.* **1956**, *78*, 5309-5311.

(51) Howard, S. T. *J. Am. Chem. Soc.* **1996**, *118*, 10269-10274.

(52) Mason, S. F. *Inorg. Chim. Acta* **1968**, *2*, 89-109.

(53) Spotswood, T. M.; Tanzer, C. I. *Aust. J. Chem.* **1967**, *20*, 1227-1242.

(54) Hazra, D. K.; Lahiri; S. C. *Anal. Chim. Acta* **1975**, *79*, 335-340.

(55) Linnell, R. H.; Kaczmarczyk, A. *J. Phys. Chem.* **1961**, *65*, 1196-1200.

(56) Irving, H.; Mellor, D. H. *J. Chem. Soc.* **1962**, 5222-5253.

(57) Irving, H.; Williams, R. J. P. *J. Chem. Soc.* **1953**, 3192-3210.

(58) Ito, T.; Tanaka, N.; Hanazaki, I.; Nagakura, S. *Bull. Chem. Soc. Japan* **1968**, *41*, 365-373.

(59) Williams, R.J.P. *J. Chem. Soc.* **1955**, 137-145.

(60) Hanazaki, I.; Nagakura, S. *Inorg. Chem.* **1969**, *8*, 648-654.

(61) Decurtins, S.; Felix, F.; Ferguson, J.; Güdel, H. U.; Ludi, A. *J. Am. Chem. Soc.* **1980**, *102*, 4102-4106.

(62) Gil, L.; Moraga, E.; Bunel, S. *Mol. Phys.* **1967**, *12*, 333-339.

(63) Hawker, P. N.; Twigg, M. V. *Comprehensive Coordination Chemistry*; Wilkinson, G.; Gillard, R. G.; Mc Cleverty, J. A. Pergamon Press: Oxford 1987; vol. 4, pp 1179-1270.

(64) Baxendale, J. H.; George, P. *Nature* **1949**, *163*, 724-725.

(65) Baxendale, J. H.; George, P. *Trans. Faraday Soc.* **1950**, 736-744.

(66) Basolo, F.; Hayes, J. C.; Neumann, H. M. *J. Am. Chem. Soc.* **1954**, *74*, 3807-3809.

(67) Margerum, D. W. *J. Am. Chem. Soc.* **1957**, *79*, 2728-2733.

(68) Krumholtz, P. *J. Am. Chem. Soc.* **1949**, *71*, 3654-3656.

Captions to Figures

Figure 1. Chemical formula of bis(2,2'bipyridine) ligand **L**.

Figure 2. Absorption spectra of ligand **L** versus iron(II) concentrations. Solvent methanol; I = 0.1 M; T = 25.0 (2)°C; a) l = 0.2 cm b) l = 2 cm; $[\mathbf{L}]_{tot} = 5.10 \times 10^{-5}$ M; p[H] = 3.50 (5); Spectra 1-11: $[Fe(II)]_{tot} \times 10^5$ M = 0.38; 0.57; 0.76; 0.95; 1.14; 1.52; 1.90; 2.28; 2.66; 3.04; 3.80 respectively.

Figure 3. ^{1}H NMR spectra of ligand **L** at different p[D]. Solvent: CD_3OD; $[\mathbf{L}]_{tot} = 10^{-3}$ M; T = 25°C.

Figure 4. Pseudo-first order rate constants $k_{1,obs}$ and $k_{2,obs}$ relative to the dissociation of $\mathbf{L}_3Fe_2^{4+}$ as a function of $[OH^-]$. Solvent: methanol; I = 0.1 M; T = 25.0 (2)°C.

Figure 5. CPK representation of ligand **L** in its best stable conformation in vacuum.

Figure 6. Formation curves of ferrous **L** complexes (a) under various acidic conditions with $[Fe(II)]_{tot}/[\mathbf{L}]_{tot} = 0.5$ or (b) under various iron(II) concentrations with p[H] = 3.50 and $[\mathbf{L}]_{tot} = 5.10 \times 10^{-5}$ M. Solvent: methanol; I = 0.1 M; T = 25 C. The stability constants are given in Table 1.

Figure 7. Self-assembling process proposed for the formation of the diferrous triple stranded helicate; S: molecule of solvent; I_2 : intermediate.

Table 1. Protonation Constants of Ligand **L** and Stability Constants of its Ferrous Complexes[a]

Thermodynamic Constant
$\log K_1 = 4.54$ (4)
$\log K_2 = 3.6$ (1)
$\log \beta_1 = 12.1$ (3)
$\log \beta_2 = 18.6$ (2)
$\log \beta_3 = 25.50$ (6)

[a]Solvent: methanol; I = 0.1 M; T = 25.0 (2)°C.

$\mathbf{L} + H^+ \underset{}{\overset{K_1}{\rightleftharpoons}} \mathbf{L}H^+$; $\mathbf{L}H^+ + H^+ \underset{}{\overset{K_2}{\rightleftharpoons}} \mathbf{L}H_2^{2+}$; $2\mathbf{L} + Fe^{2+} \underset{}{\overset{\beta_1}{\rightleftharpoons}} \mathbf{L}_2Fe^{2+}$; $2\mathbf{L} + 2Fe^{2+} \underset{}{\overset{\beta_2}{\rightleftharpoons}} \mathbf{L}_2Fe_2^{4+}$; $3\mathbf{L} + 2Fe^{2+} \underset{}{\overset{\beta_3}{\rightleftharpoons}} \mathbf{L}_3Fe_2^{4+}$

Table 2. Dissociation Mechanism of the Helicate $\mathbf{L}_3Fe_2$: Thermodynamic and Kinetic Parameters[a]

Rate Constant (s^{-1})	Equilibrium Constant (M^{-1})
	$K_1 = 2.2$ (5)
	$K_2 = 18$ (4)
$k_3 = 0.19$ (4)	
$k_{d,\mathbf{L}_3Fe_2} = 4$ (2) $\times 10^{-4}$	
	$K_4 = 3.1$ (7)
	$K_5 = 16$ (4)
$k_6 = 4.9$ (9) $\times 10^{-2}$	
$k_{d,\mathbf{L}_3Fe} = 7$ (2) $\times 10^{-5}$	

[a]Solvent: methanol; I = 0.1 M; T = 25.0 (2)°C. Charges are omitted for the sake clarity.

Table 3. Protonation Constants of 2,2'-bipyridine and Substituted Analogues at 25°C.

Ligand	log K_1
2,2'-bipyridine	4.47[a]
	3.04[b]
	3.62[c]
5,5'-$(CH_3)_2$ 2,2'-bipyridine	3.97[c]
5,5'-$(CO_2C_2H_5)_2$ 2,2'-bipyridine	0.85[c]

[a] Water;[43] [b] Methanol:water (87.9% by weight)[43]; [c] Dioxane:water (50:50)[45].

$$L + H^+ \underset{\longleftarrow}{\xrightarrow{K_1}} LH^+$$

Table 4. Absorption Maxima of the Different Protonated Species and Ferrous Complexes of Ligand **L** and 2,2'-bipyridine[49,55,68] at 25°C.

Species	λ_{max} (nm)	ε_{max} (M^{-1} cm^{-1})
2,2'-bipyridine	282	13000
mono protonated 2,2'-bipyridine	302 shoulder 315	15800
diprotonated 2,2'-bipyridine	290	15500
(2,2'-bipyridine)Fe^{2+}	435	310
(2,2'-bipyridine)$_2Fe^{2+}$	500	300
(2,2'-bipyridine)$_3Fe^{2+}$	523	8500
L	291	45200 (100)
$\mathbf{LH}^+$	305 shoulder 320	39700 (300)
$\mathbf{LH_2}^{2+}$	309 shoulder 320	51100 (300)
$\mathbf{L_2Fe}^{2+}$	308 526	35200 (1900) 5900 (200)
$\mathbf{L_2Fe_2}^{2+}$	305 540	124000 (12000) 7800 (600)
$\mathbf{L_3Fe_2}^{4+}$	305 540	166500 (3700) 15300 (350)
$\mathbf{L_3Fe}^{2+}$	305 540	137000 (14000) 8400 (900)

The errors on λ are estimated to ± 2 nm

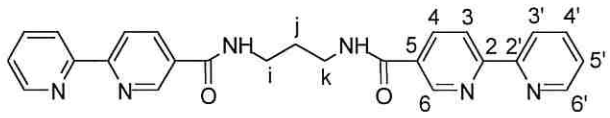

Figure 1

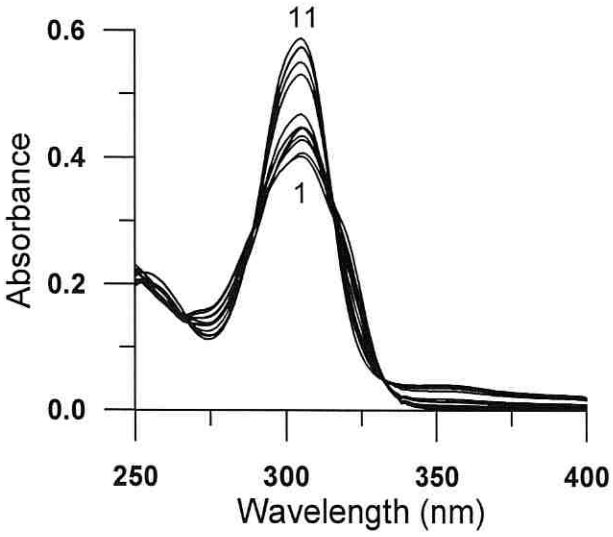
11
1
0.6
0.4
0.2
0.0
Absorbance
250
300
350
400
Wavelength (nm)

a)

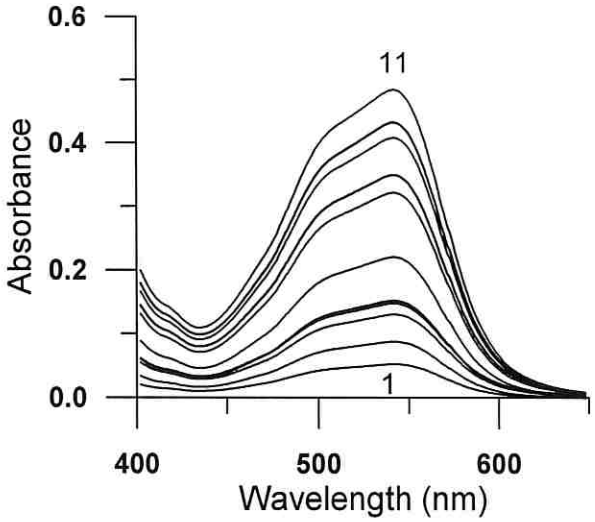
11
1
0.6
0.4
0.2
0.0
Absorbance
400
500
600
Wavelength (nm)

b)

Figure 2

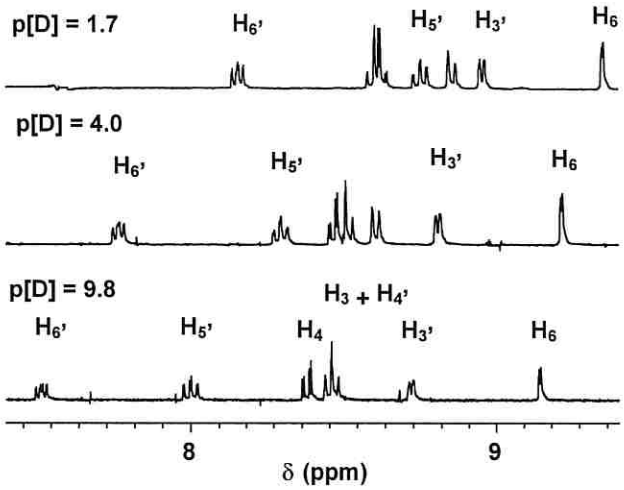

Figure 3

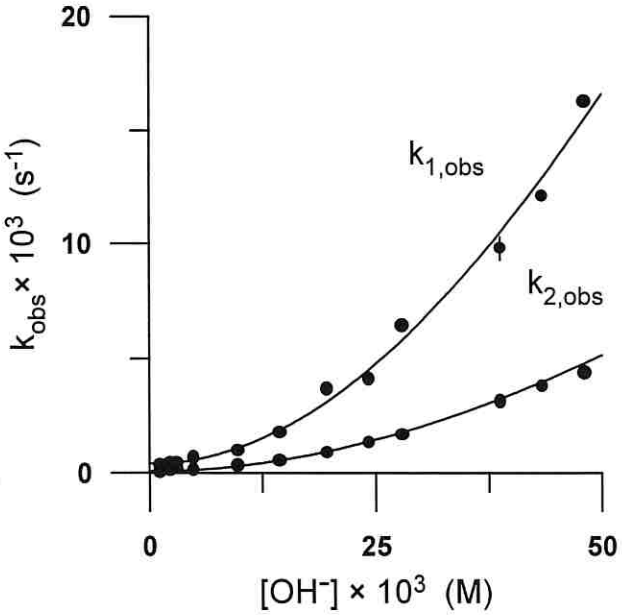

Figure 4

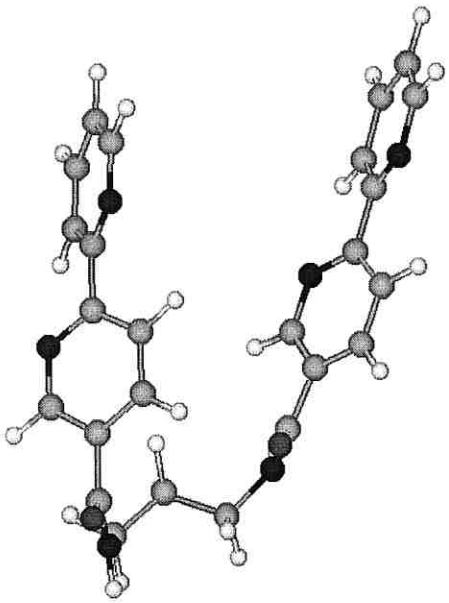

Figure 5

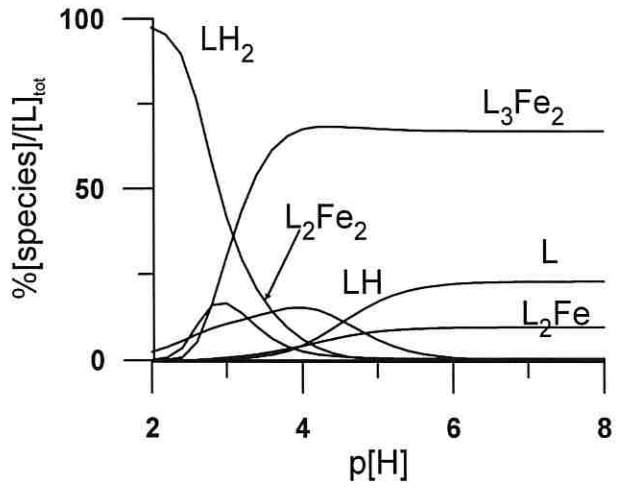
100
50
0
%[species]/[L]tot
LH2
L3Fe2
L2Fe2
L
LH
L2Fe
2
4
6
8
p[H]

a)

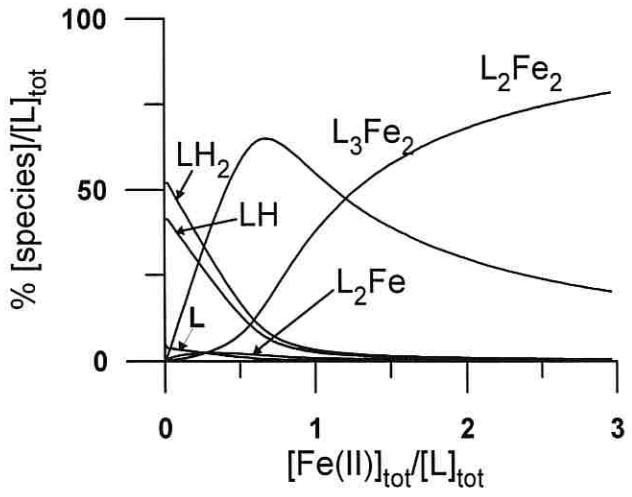
100
50
0
% [species]/[L]tot
L2Fe2
L3Fe2
LH2
LH
L2Fe
L
0
1
2
3
[Fe(II)]tot/[L]tot

b)

Figure 6

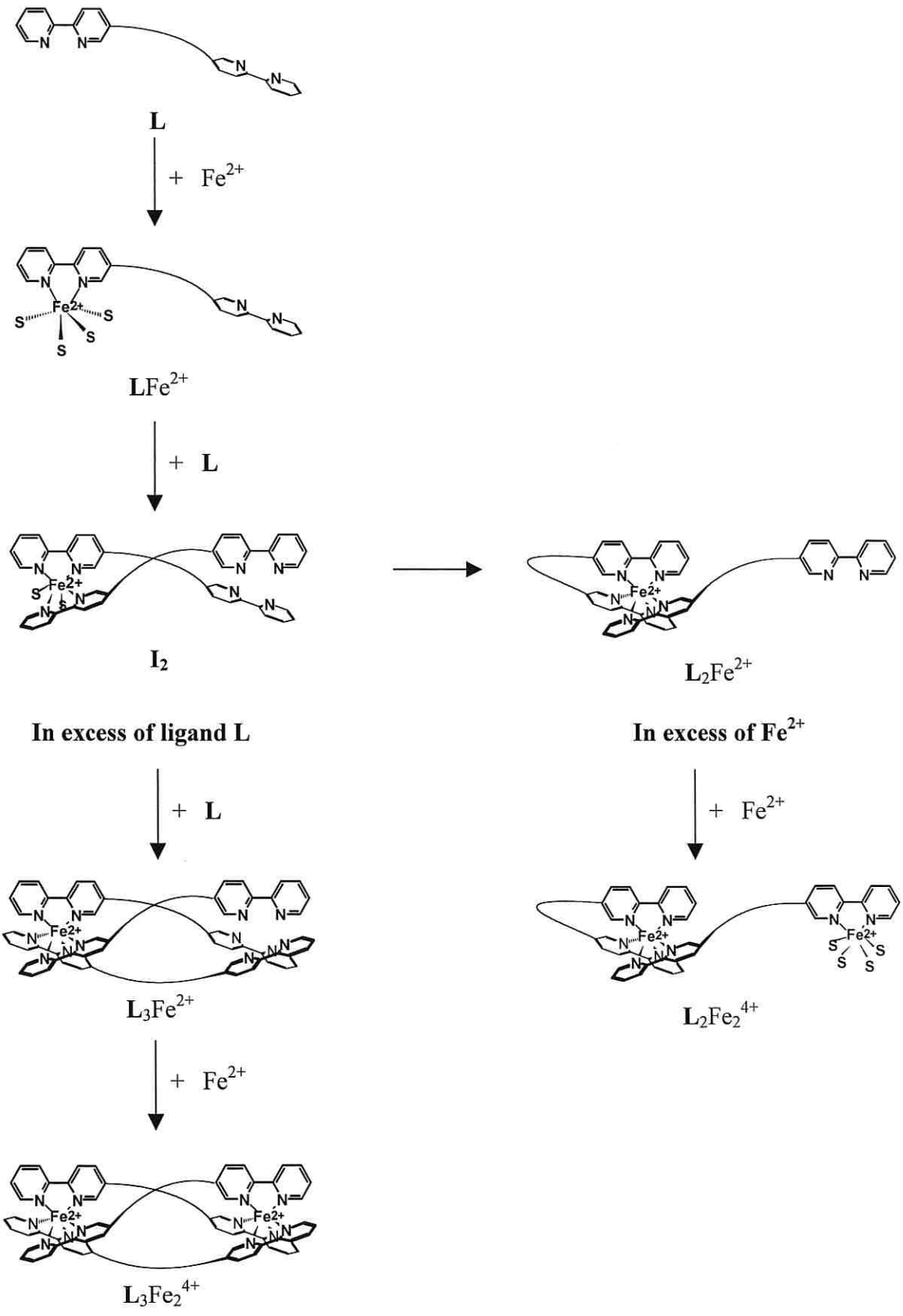
L
+ Fe2+
LFe2+
+ L
I2
L2Fe2+
In excess of ligand L
In excess of Fe2+
+ L
+ Fe2+
L3Fe2+
L2Fe2 4+
+ Fe2+
L3Fe2 4+

Figure 7